Earth and Planetary Science Letters 335–336 (2012) 226–237

Contents lists available at SciVerse ScienceDirect

Earth and Planetary Science Letters

journal homepage: www.elsevier.com/locate/epsl

Consequences of mantle heterogeneity for melt extraction at mid-ocean ridges

Richard F. Katz *, Samuel M. Weatherley

Department of Earth Sciences, University of Oxford, South Parks Road, Oxford OX1 3AN, United Kingdom

ARTICLE INFO

Article history:
Received 15 October 2011
Received in revised form
7 March 2012
Accepted 14 April 2012
Editor: L. Stixrude

Keywords:
mid-ocean
ridge
magmatism
mantle
heterogeneity
eclogite

ABSTRACT

Evidence for chemical heterogeneity of the mantle is found at most mid-ocean ridges, yet we are only beginning to develop a theoretical understanding of how this heterogeneity affects basalt petrogenesis. In particular, the consequences of heterogeneity for magma transport through the mantle are not known. We address this question with computational models of coupled magma/mantle dynamics and thermochemistry beneath ridges. The models are initialised with simple, hypothetical patterns of mantle heterogeneity; we investigate the consequences of this heterogeneity for the predicted pathways of melt transport. Our results show that preferentially melted heterogeneities can nucleate magmatic channels that transport their melts. A channel generated in this way is cooler than the surrounding mantle; the temperature gradient drives an inward diffusive flux of heat, powering melting within and suppressing melting on its flanks. The channels become high-porosity, high-permeability pathways for rapid magmatic ascent toward the surface. Channelised flow has implications for the extent of mixing between melts that are derived from distinct sources. Melt segregation from the heterogeneous source in our models creates pools of trapped melt at the base of the lithospheric boundary layer, away from the ridge axis; these pools freeze and introduce new heterogeneity into the mantle. They may also deliver melt via dikes to off-axis magma chambers in the crust.

1. Introduction

It is recognised that basalt petrogenesis in all tectonic settings occurs by partial melting of a chemically and lithologically heterogeneous mantle source. Evidence for this heterogeneity, in the form of recycled oceanic crust, comes from petrology (Hofmann and White, 1982; Hirschmann and Stolper, 1996; Hauri, 1996; Shorttle and Maclennan, 2011), seismology (Helffrich and Wood, 2001; Ritsema et al., 2009), and a consideration of the history of crustal subduction (Davies, 2009). Furthermore, there is increasing recognition of the critical role that melt transport plays in preserving or destroying chemical variability that is inherited from a heterogeneous mantle source (Maclennan, 2008; Stracke and Bourdon, 2009; Liang et al., 2011). Progress in the interpretation of geochemical observations in terms of mantle heterogeneity must therefore be coupled with progress in physical models for melt transport. While there is much prior work on the fluid dynamics of melt extraction, and it was recognised early that these dynamics are affected by mantle heterogeneity (Richter and Daly, 1989), no previous model has explicitly incorporated chemical and lithological heterogeneity. Here we use mathematical models of coupled magma/mantle dynamics and thermochemistry to address this challenge. We investigate the consequences of mantle heterogeneity for magmatic transport beneath mid-ocean ridges. Our results suggest that previous models may have missed important aspects of magmatism.

Recent interest in magmatic transport has focussed on the observation that mid-ocean ridge basalt (MORB) is not in equilibrium with orthopyroxene-bearing rocks at Moho pressures, despite the existence of harzburgite and lherzolite there. Instead, MORB-forming melts are undersaturated in orthopyroxene. An explanation for this was developed based on the structure of the Oman ophiolite, where the exhumed mantle has alternating bands of harzburgite and dunite. Kelemen et al. (1995) proposed that a substantial portion of melt is transported from depth through high-porosity channels, and that this melt reacts with the mantle, stripping out pyroxene until the solid residuum is entirely olivine. Subsequent melt that travels through the dunite is chemically isolated from the surrounding harzburgite, and remains undersaturated in orthopyroxene. Chemical isolation during transport can also preserve the trace-element and isotopic signature inherited by melts at depth, as they ascend to the surface (e.g. Kelemen et al., 1995; Lundstrom et al., 2000;

* Corresponding author. Tel.: +44 1865 282122.
E-mail address: richard.katz@earth.ox.ac.uk (R.F. Katz).
URL: http://foalab.earth.ox.ac.uk (R.F. Katz).

0012-821X/$ - see front matter © 2012 Elsevier B.V. All rights reserved.
http://dx.doi.org/10.1016/j.epsl.2012.04.042

Jull et al., 2002; Spiegelman and Kelemen, 2003; Elliott and Spiegelman, 2003). Furthermore, the enhanced permeability associated with channelised flow may reconcile porous melt-transport theory (McKenzie, 1984) with geochemical and geological observations indicating rapid melt extraction (e.g. Kelemen et al., 1997; Maclennan et al., 2002; Stracke et al., 2006).

To model this system, Aharonov et al. (1995) proposed a theoretical framework that couples a formulation for reactive flow up a solubility gradient with the canonical equations for porous melt-transport and compaction (McKenzie, 1984). Their analysis showed that when upwelling magma drives reactive melting of the host rock, a fluid-mechanical instability can transform the diffusely distributed magmatic flow into high-porosity channels surrounded by compacted, low-porosity regions. The channels transport most of the magmatic flux. This flux drives an incongruent melting reaction (Morgan and Liang, 2003), and together this hypothetically gives rise to the pattern of dunite and harzburgite domains observed in ophiolites (Spiegelman and Kelemen, 2003; Liang et al., 2010).

Mantle heterogeneity has received scant attention in these studies, which have generally considered an initially uniform mantle modified by vanishingly small random perturbations (Aharonov et al., 1995; Spiegelman et al., 2001; Spiegelman and Kelemen, 2003). Even Schiemenz et al. (2011), who emphasised mantle heterogeneity in the title of their paper, actually considered a chemically homogeneous mantle source. That study imposed a spatially fixed perturbation to porosity at the bottom (inflow) boundary, resulting in the emergence of a channel directly above. This emergence can be loosely interpreted as channel growth above an anomalously fertile source. However, the formulation of Schiemenz et al. (2011) includes neither compositional variation in melts and solids, nor the time dependence that arises from advection of the fusible heterogeneity through the melting region.

More importantly, most previous work on reactive melting and channelised flow has neglected the energetics of the system (Aharonov et al., 1995; Spiegelman et al., 2001; Liang et al., 2010; Schiemenz et al., 2011). Mantle melting is an inherently thermodynamic process; theoretical models that predict melting rates without accounting for conservation of energy are inconsistent. Recent, energy-conservative simulations and stability analysis by Hewitt (2010) indicate that magmatic channels do not emerge within a homogeneous mantle. His calculations capture both flux and decompression melting in a thermodynamically consistent manner, and are hence a more accurate representation of the natural system than previous models. They present a challenge to the prior understanding of the emergence of channelised melt transport developed by Aharonov et al. (1995) and Spiegelman et al. (2001). Relevant to the present study, Hewitt (2010) also showed that an excess flux of melt into the bottom of the mantle melting regime can induce channelisation, even under conservation of energy. We hypothesise that this excess flux of melt is derived from melting of fertile, recycled crustal materials at depths between about 60 and 120 km.

The models reviewed above vary in whether they assume local thermodynamic equilibrium between phases. There is no consensus on the length or time-scale over which major-elements equilibration occurs between magma and solid mantle. The assumption of chemical equilibrium in magmatic reactive-flow models does seem to affect the qualitative behaviour of the models, however. Spiegelman et al. (2001) modelled a disequilibrium system with linear kinetics and considered different reaction-rate constants; to initiate channels, they applied a vanishingly small perturbation to the melting rate on the grid scale. Their models showed a decrease in the width and spacing of channels with increasing reaction rate. Liang et al. (2010) and Schiemenz et al. (2011) considered a similar model but with infinite reaction rate (i.e. thermodynamic equilibrium), and applied a perturbation of finite width and amplitude in the input magmatic flux. Their focus was on the structure and dynamics of a single or a pair of channels. Both Spiegelman and Kelemen (2003) and Schiemenz et al. (2011) considered incongruent melting with two solid phases (olivine and pyroxene), whereas Hewitt (2010) and this study assume a single solid phase in chemical and thermal equilibrium with the magma. Without controlled numerical experiments or theoretical developments, it is impossible to isolate the effects of specific assumptions with confidence. A parameter study in a companion to the present paper (Weatherley and Katz, 2012) attempts to address this deficiency, but there is much more that could be done.

In the present manuscript, we build on the simulations of mid-ocean ridges described by Katz (2010) by introducing hypothetical distributions of chemical heterogeneity in the simulated mantle. The actual chemical variation within the mantle is poorly known, in terms of its amplitude, length-scales, and interconnectivity. Models of convective stirring predict that heterogeneity should appear as tabular veins on a range of scales (Allègre and Turcotte, 1986), but it is not clear whether there is equal chemical variation "on all observable spatial scales" ($\gtrsim 5$ km) (Gurnis, 1986), or if there are one or more characteristic scales (Kogiso et al., 2004; Helffrich and Wood, 2001). Furthermore, there is an ongoing debate regarding how heterogeneity is incorporated into the source of erupted basalts: Sobolev et al. (2007) argue that global geochemical observations of lavas require melting of a source that includes an olivine-free hybrid pyroxenite (peridotite refertilised by reaction with melts derived from recycled crust, Yaxley and Green, 1998). In contrast, geochemical models by Shorttle and Maclennan (2011) of data from Icelandic lavas do not require an olivine-free lithology. Rather, they argue that the source is composed of depleted and refertilised peridotite, the latter incorporating about 40% recycled mid-ocean ridge basalt.

A variety of constraints exist for the fraction of fertile material in the source regions of mid-ocean ridge magmas. Roughly consistent estimates of 5–15% are derived from simple reservoir models (Davies, 2009), petrological considerations (Pertermann and Hirschmann, 2003; Shorttle and Maclennan, 2011), regional geochemical indicators (Sobolev et al., 2007), and more comprehensive geochemical inversions (Ito and Mahoney, 2005). Given these broad constraints (and the limits of what is computationally feasible), we investigate two possible scenarios for mantle heterogeneity using a petrological model that describes melting of a single lithology, with spatial variation in source fertility.

As in precursory work, we couple the canonical formulation for magma/mantle dynamics (McKenzie, 1984) with a consistent, energy-conserving, thermochemical model of melting (Katz, 2008). Our purpose here is to describe a few basic but significant results from the model. A more in-depth analysis is provided in a companion paper (Weatherley and Katz, 2012), and there are many related avenues to explore in the future work. The theoretical framework for the present results is described qualitatively in the following section; mathematical details are available in the previous publications (Katz, 2008, 2010). Section 3 explores representative calculations for two model systems: first, a two-dimensional mid-ocean ridge domain with large-scale mantle deformation, and second, a two-dimensional upwelling column in which deformation is restricted to compaction/decompaction. A discussion of the results is given in Section 5; we draw some tentative conclusions in Section 6.

2. Theory and methods

The mathematical theory and numerical solutions considered here are an extension of previous work with two-phase models of

mid-ocean ridges (MORs) (Katz, 2008, 2010). These use a continuum representation of two interpenetrating fluids with contrasting properties: the mantle is a crystalline solid that undergoes creeping flow, the magma is a liquid that moves through the interconnected pore-spaces between mantle grains (e.g. McKenzie, 1984). Requirements of conservation of mass, momentum, and energy for both phases and two thermochemical components give rise to a system of coupled, nonlinear, partial differential equations. For the full MOR simulations presented below, the fluid mechanics are identical to that considered in Katz (2010). The only difference between Katz (2010) and present simulations is that here, magma that rises to the ridge axis is not extracted—rather, it is allowed to pool and crystallise, creating a fertile layer that corresponds to the oceanic crust at the top of the domain.

A consistent thermochemical description of melting is a key aspect of the present models. Most previous work has used a mathematical formulation of disequilibrium magmatic flow that is independent of temperature. This approach typically asserts a two-component melting model with linear kinetics: the melting rate is proportional to the compositional difference from equilibrium. A more general and thermodynamically rigorous formulation was developed by Rudge et al. (2010), but has not been implemented as part of a geodynamic simulation. We adopt the assumption of chemical equilibrium between magma and solid mantle, but we account also account for the energetics of the system, following on the work of Ribe (1985), Katz (2008, 2010), and Hewitt (2010). Our formulation is based on the assumption of thermodynamic equilibrium in a two-phase (solid mantle+liquid magma), two-component system that is described by a linearised phase diagram (Fig. 1). By the conventional definition, the fertile component has a low melting temperature, while the refractory component melts at a higher temperature; all simulated compositions are a mixture of these two components. The phase diagram is applied at every grid cell in the domain to compute the temperature, volume fraction of melt (porosity), and composition of each phase from the bulk enthalpy and bulk composition

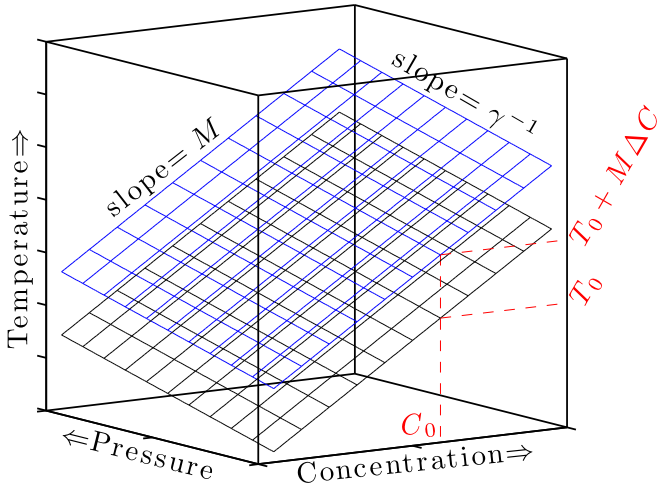

Fig. 1. Phase diagram showing the relationship of solidus temperature (black) and liquidus temperature (blue) to pressure and concentration of the refractory component. The solidus surface is given as $T = T_0 + \gamma^{-1}P + M(C_m - C_0)$, where $T_0 = 1300\ ^\circ$C and $C_0 = 0.85$ wt.frac. are reference values at $P = 0$, $M = 400\ ^\circ$C/wt.frac. is the solidus slope with concentration, $\gamma^{-1} = 60\ ^\circ$C/GPa is the Clapeyron slope, and C_m is the concentration of the refractory component in the solid phase. The liquidus surface is given by the same equation but with $C_f = C_m - \Delta C$, where C_f is the concentration of the refractory component in the liquid phase and ΔC is the distance between the two surfaces along the concentration-axis. This is the simplest petrologic model that can capture the fundamental aspect of mantle heterogeneity, namely the solidus contrast between fertile ($C_m < C_0$) and refractory ($C_m > C_0$) rocks. (For interpretation of the references to colour in this figure caption, the reader is referred to the web version of this article.)

at that grid cell. Because the governing equations are discretised by a finite-volume method, the bulk enthalpy and composition are cell-averaged values; this implies an equilibration length that is approximately equal to the grid spacing (~ 750 m). In the mantle, we expect that thermochemical variations are smooth, but may be present on scales smaller than we resolve; high-resolution discretisations (e.g. Schiemenz et al., 2011) have proven to be valuable for modelling of channelised flow and should be extended to consider thermodynamically consistent formulations of the governing physics.

The initial mantle composition in our models is a hypothetical mantle-heterogeneity field that is generated using one of the two stochastic algorithms. The first of these produces a random array of fertile blobs with a given size-range; the second produces a random noise-field with given spectral properties (see Appendix A for full details). The array of fertile blobs produced by the random-blob algorithm makes up a specified area fraction of the domain (10% in Fig. 2a). The blobs are initially uniform, have sharp edges (compared to the grid scale), and are embedded in an ambient mantle with uniform composition. They are approximately equant relative to the predicted shape of heterogeneities that have been transported through plume conduits (Farnetani and Hofmann, 2009), though the simulated flow field in the present ridge models does lead to stretching with time. The blobs are topologically isolated rather than interconnected, which has implications for predicted patterns of melt transport. These choices are driven, in part, by limitations of the discretisation in resolving advection of filamentous structures. Despite such shortcomings, the random blob hypothesis is a relevant end-member for melting and melt transport through a heterogeneous mantle.

Heterogeneities beneath a mid-ocean ridge that have been stirred or reacted into the mantle at a length-scale much finer than 1 km cannot be resolved individually in a ridge-scale model. Our second hypothesis therefore posits a mixture with spatially variable concentration of recycled material. This concentration may be considered to represent peridotite variably refertilised by reaction with recycled basalt, or it may represent a grid-scale average of the fraction of sub-grid-scale basaltic veins. The associated algorithm produces a random variation of concentration with a specified power-spectrum, chosen to control the smoothness of the heterogeneity field (Fig. 2b). Under this hypothetical scenario, variation initially exists at every scale, from the grid scale to the domain scale. The magnitude of variation at each scale is given by the slope on a plot of log-spectral variance versus log-frequency.

The upwelling-column models that are presented below use a reduced mechanical theory that excludes large-scale shearing flow. In this case, the mantle velocity is given by $\mathbf{v}_m = -W_0\hat{\mathbf{g}} + \boldsymbol{\nabla}\mathcal{U}$, where $\hat{\mathbf{g}}$ is a unit-vector pointing in the direction of gravity, $W_0 > 0$ is the speed of mantle upwelling through the column, and $\mathcal{U}$ is the compaction potential, which we obtain as part of the numerical solution. This formulation for modelling a mantle upwelling column has been used in a variety of studies, including Spiegelman and Kelemen (2003), Hewitt (2010), and Liang et al. (2010).

For both full MOR and upwelling-column models, the governing equations are discretised using a finite-volume method on a fully staggered grid. The resulting nonlinear algebraic system is solved within the framework of the Portable, Extensible Toolkit for Scientific Computation (PETSc, Balay et al., 2011), using parallel computers. See Appendix C and Katz (2010) for further details.

3. Results

In this section we present representative results from two mid-ocean ridge simulations. The channelisation behaviour observed in

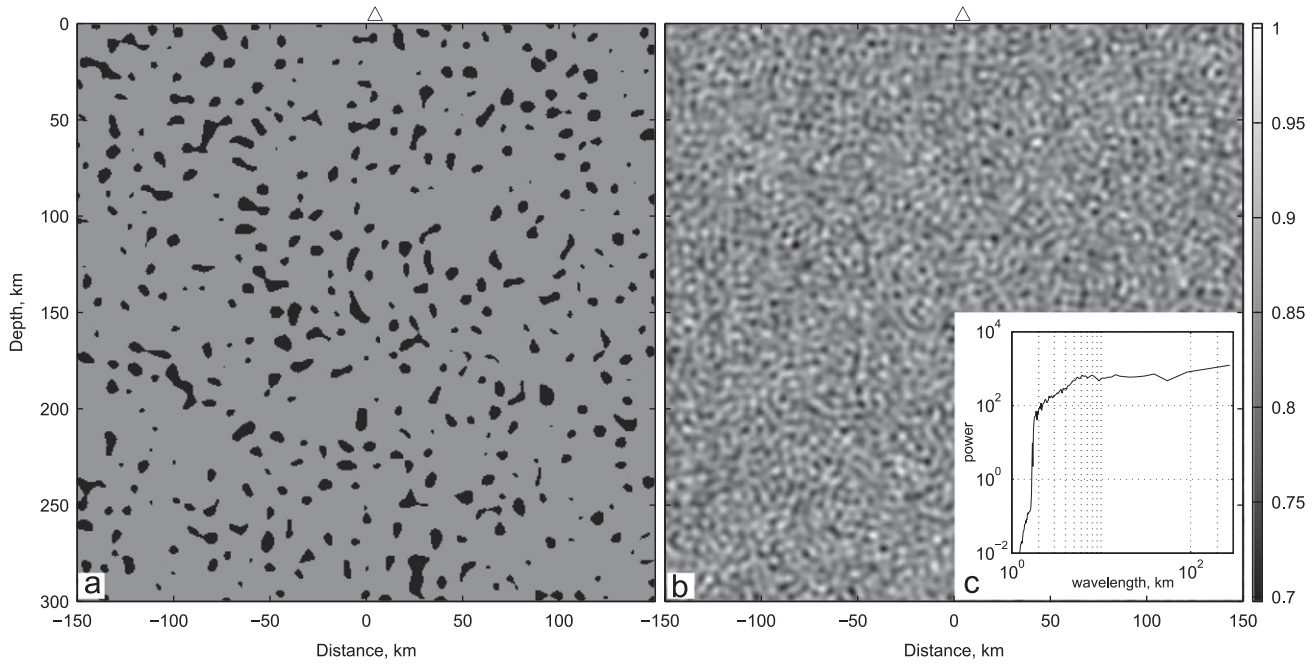

Fig. 2. The initial mantle heterogeneity pattern used in the ridge simulations presented below. The background mantle composition is $C_0 = 0.85$ wt.frac. for both panels. These fields are used to initialise the calculation, and as a "reservoir" beneath the domain to supply unmolten, heterogeneous mantle. The governing equations are solved within the domain marked by the white dashed line; in figures below, only the subregion within the black dashed line is shown. Unmolten mantle is advected into the domain from the reservoir below. The field in panel (a) was created using the random blob algorithm with 10% fertile fraction, and that in (b) was created using the random noise algorithm with a minimum wavelength of about 2 km. The compositional perturbation is $C_* = 0.15$, corresponding to a solidus perturbation of 60 K. Both panels use the same colour bar and have the same mean concentration; (b) has greater variation because it has enrichment and depletion by C_*. Panel (c) plots the directionally averaged spectral power of the two-dimensional noise field in panel (b), showing approximately uniform power above a wavelength of 5 km and a drop-off in power below 5 km. Details of the algorithms used to generate the heterogeneity fields are given in Appendix A.

Table 1
Parameters and their values as used in the simulations reported here. These are chosen from within accepted ranges to give larger melt extraction rates. The sensitivity to parameter variation is considered by Weatherley and Katz (2012).

Quantity	Symbol	Value used	Units
Shear viscosity	η_0	10^{19}	Pa s
Bulk viscosity	ζ_0	2×10^{19}	Pa s
Permeability constant	K_0	10^{-7}	m^2
Permeability exponent	n	3	
Fluid viscosity	μ	1	Pa s
Density	ρ	3000	kg/m^3
Density difference	$\Delta\rho$	500	kg/m^3
Specific heat capacity	c	1200	J/kg/K
Gravity	g	9.8	m/s^2
Thermal diffusivity	κ	10^{-6}	m^2/s
Chemical diffusivity/dispersivity	$\mathcal{D}$	10^{-8}	m^2/s
Thermal expansivity	α	3×10^{-5}	K^{-1}
Latent heat	L	4×10^5	J/kg
Clapeyron slope	γ	1.7×10^7	Pa/°C
Solidus and liquidus slope	M	400	K/wt.frac.
Mantle potential temperature	$\mathcal{T}_0$	1375	°C
Reference melting temperature	T_0	1300	°C

these calculations is examined in more detail in an upwelling-column model. Parameter values used in the calculations are given in Table 1.

3.1. Mid-ocean ridge models

Fig. 3 shows a time-slice of mantle composition, porosity, and temperature fields from two representative simulations (links to animations are in Appendix B). The simulations have equal parameter values, but different initial mantle-heterogeneity fields. In the left column, the mantle source contains a stochastically generated array of fertile blobs, comprising an area fraction of 10%. The blobs are initially of uniform composition and, at any pressure, have a solidus that is 60 K lower than the solidus temperature of the ambient mantle. In the right column, the mantle source has a smoothed, random variation in composition, with an amplitude of ± 60 K in solidus temperature. Both heterogeneity fields have the same mean fertility.

These results should be compared with simulations that have a homogeneous mantle but are otherwise equivalent (e.g. Katz, 2008, 2010). In the homogeneous case we obtain a roughly triangular melting regime, free from channels, and delineated by the area where mantle is both upwelling and above its solidus temperature. Sub-ridge mantle upwelling for a two-dimensional, homogeneous case is symmetrical about the ridge axis, and is typically assumed to be close to the corner-flow solution of Batchelor (1967).

The mantle composition, plotted in panels a and d, is coloured according to the associated variation of the solidus temperature. Cold colours represent fertile compositions, and hence reduced solidus temperature; warm colours represent refractory compositions with higher solidus temperature. The colour scale is proportional to $\Delta T_C = M(C_m - C_0)$, where M is the solidus slope with respect to composition, C_m is the solid composition, and C_0 is a constant reference composition. ΔT_C is therefore the difference in the melting temperature of the solid with respect to the ambient (or mean) upper mantle composition. There is greater depletion evident in panel d than in panel a because the initial heterogeneity field is composed of variations both more fertile and more refractory than the background. The initial heterogeneity fields, before they are modified by melting and melt transport, are shown in Fig. 2.

The porosity field for the ridge models is shown in panels b and e. The heterogeneous composition gives rise to a

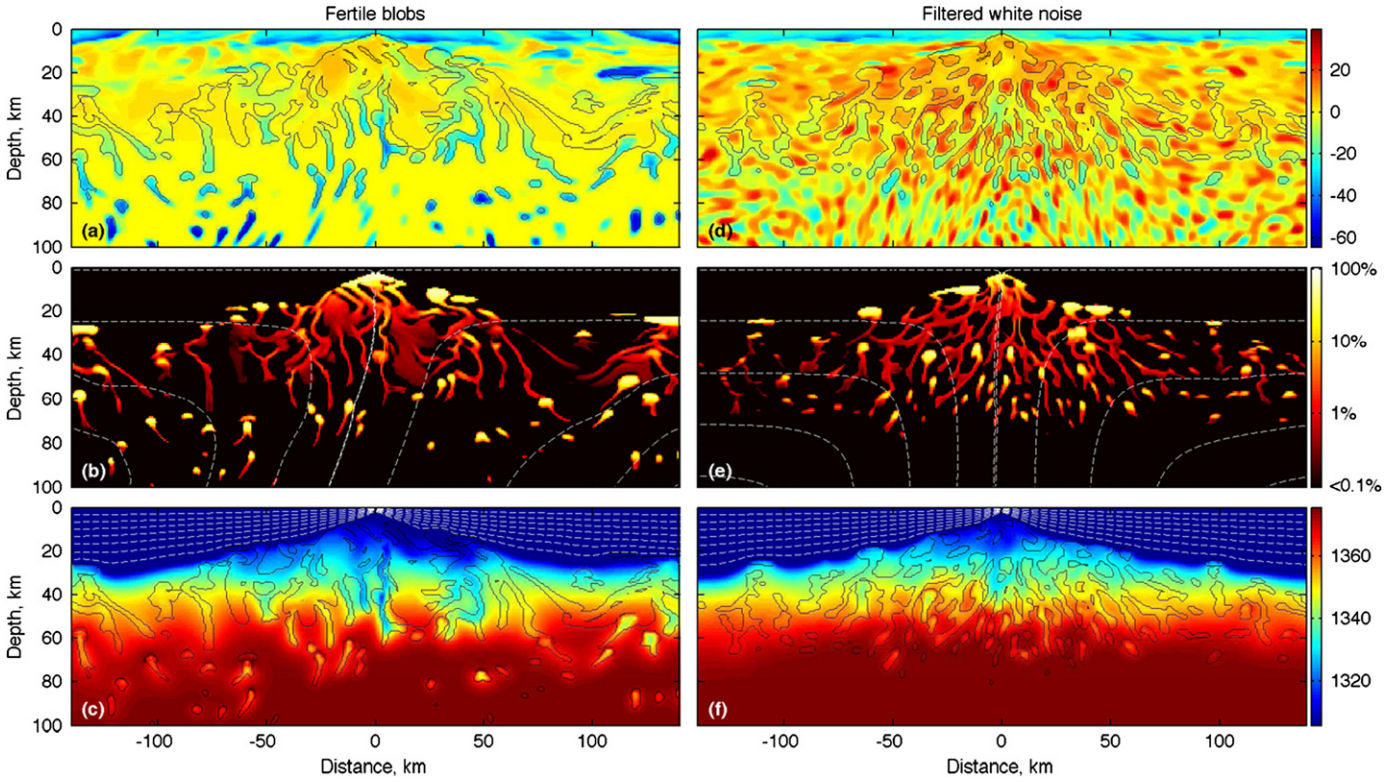

Fig. 3. Representative output from two ridge simulations with a half-spreading rate of 4 cm/a. Panels (a) and (d) show the compositional perturbation of solidus temperature $\Delta T_C = M(C_m - C_0)$ in °C, as a physical proxy for chemical heterogeneity. The boundary between partially molten and unmolten mantle is delineated in black. The fertile layer at the top of the domain represents the oceanic crust. It is produced by solidification within the simulated axial magma chamber. Panels (b) and (e) show the porosity field with a log-scale colour-bar; porosities below 0.1% are shown as black. Mantle streamlines are overlain in white. Panels (c) and (f) show the mantle potential temperature, with a colour-scale chosen to highlight temperature variability in the asthenosphere. Temperature contours within the lithosphere are overlain in white. The grid-spacing is 0.75 km in both simulations. Initial heterogeneity fields are shown in Fig. 2. Movies of these simulation results are in the Supplementary materials. (For interpretation of the references to colour in this figure caption, the reader is referred to the web version of this article.)

heterogeneous distribution of porosity that, in turn, is associated with a heterogeneous distribution of buoyancy. This buoyancy drives convection, breaks the symmetry of corner-flow, and introduces localised, off-axis upwelling. Fertile mantle blobs melt at depth and retain their melt until they merge with the ambient melting regime. When this connection is established, the magma rises rapidly from the blob, leading to reactive melting and, in some cases, channelised flow. Overall, the channels coalesce upward and empty into high-porosity pools at the base of the thermal boundary layer. The largest of these pools is located immediately beneath the ridge axis, but others appear off-axis as well, where magma becomes trapped beneath the lithosphere. In these sub-lithospheric melt pools, and within the fertile heterogeneities before their melt escapes, the porosity reaches values that exceed the disaggregation fraction ($\gtrsim 20\%$, McKenzie, 1984; Hier-Majumder et al., 2006). The governing equations for force-balance assume contiguity of the solid phase, and are therefore invalid under these high-porosity conditions, though the mass and energy-conservation equations remain valid. Section 4 includes a discussion of this issue.

Although the porosity field in panels b and e of Fig. 3 both show large spatial variations, the two hypothetical distributions of mantle heterogeneity produce subtly different results. The isolated blobs of fertile mantle (panel b) release magma into the moderately refractory ambient mantle rock that surrounds them. This tends to produce narrow channels that are initially vertical. The channels may connect with other fertile source-regions, or they may simply grow into a region of refractory composition. In simulations initiated with random noise (panel e), the distribution of heterogeneity has a different topological configuration: fertile regions interconnect with other fertile regions because the concentration varies smoothly in the source. Melt extraction therefore occurs by transfer along pathways between fertile regions. In general, these pathways are not oriented vertically, so magma can take a meandering upward route.

The temperature field shown in Fig. 3c and f also includes features that arise from the spatial structure of chemical heterogeneity. Because heterogeneities and their attendant channels have more fertile compositions than the surrounding mantle, they melt at a lower temperature; sensible heat from the ambient mantle therefore diffuses into them, powering melting in excess of that due to decompression (Sleep, 1984; Katz and Rudge, 2011). This coupled process of melting and thermal diffusion produces a halo of reduced temperatures around blobs and channels; mantle melting is suppressed within this halo. The energy converted to latent heat during melting is restored to sensible heat when magma crystallises. Dashed lines in Fig. 3c and f are temperature contours within the lithosphere. These lines deviate from a conductive cooling solution near the base of the lithosphere, where melt accumulates as trapped pools. Crystallisation in these locations releases sensible heat, which buffers the temperature and hence locally modifies the thermal structure.

Fig. 4 shows the melting rate Γ (panels a and c) and the magmatic flow rate (panels b and d) from the same two simulations as in Fig. 3. The melting rate is calculated diagnostically from subsequent time-steps according to a discretised version of the non-dimensional mass conservation equation, $\Gamma = \partial_t \phi - \nabla \cdot (1-\phi)\mathbf{v}_m$, where ∂_t is the partial derivative with respect to time, ϕ is the porosity, and $\mathbf{v}_m$ is the mantle velocity. This equation states that the melting rate is given by the change in porosity

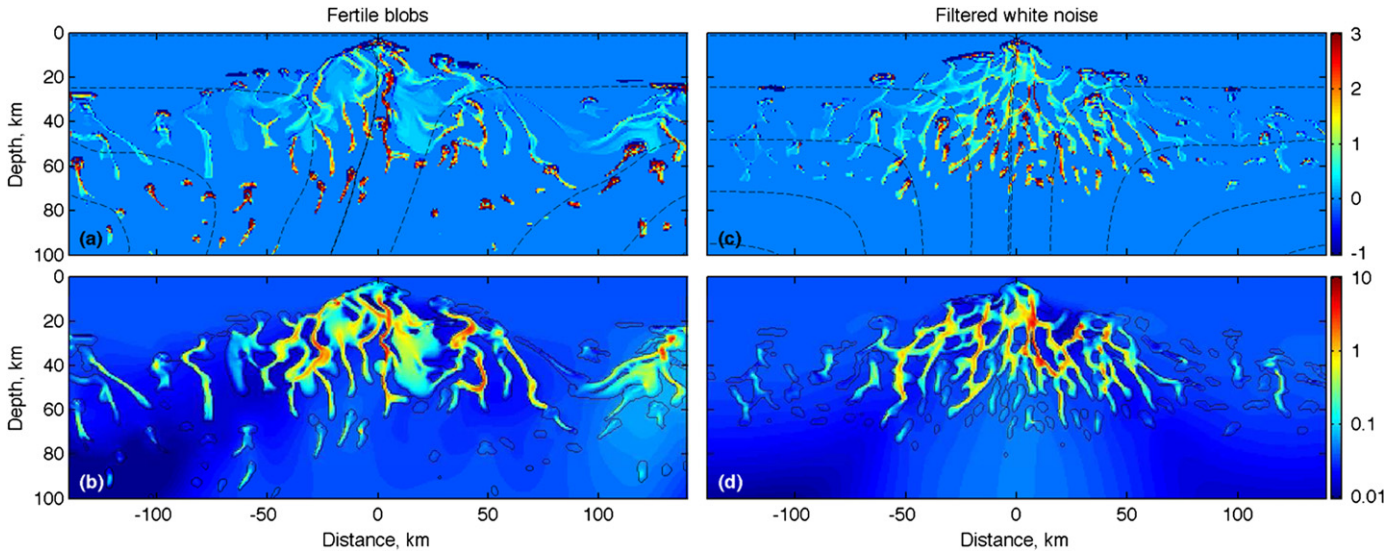

Fig. 4. Melting rate and magmatic flow speed for the same two simulations and the same model time as the output shown in Fig. 1 of the main paper. The left-column simulation was initiated with a random array of fertile blobs, while the right-column simulation was initiated with a smoothed, random-noise field. Panels (a) and (c) show the melting rate Γ in units of 10^{-3} kg/m^3/yr. Panels (b) and (d) show the magnitude of the magma velocity in units of m/yr. Note that the colour scale is logarithmic in the velocity. Movies of these simulation results are in the Supplementary materials. (For interpretation of the references to colour in this figure caption, the reader is referred to the web version of this article.)

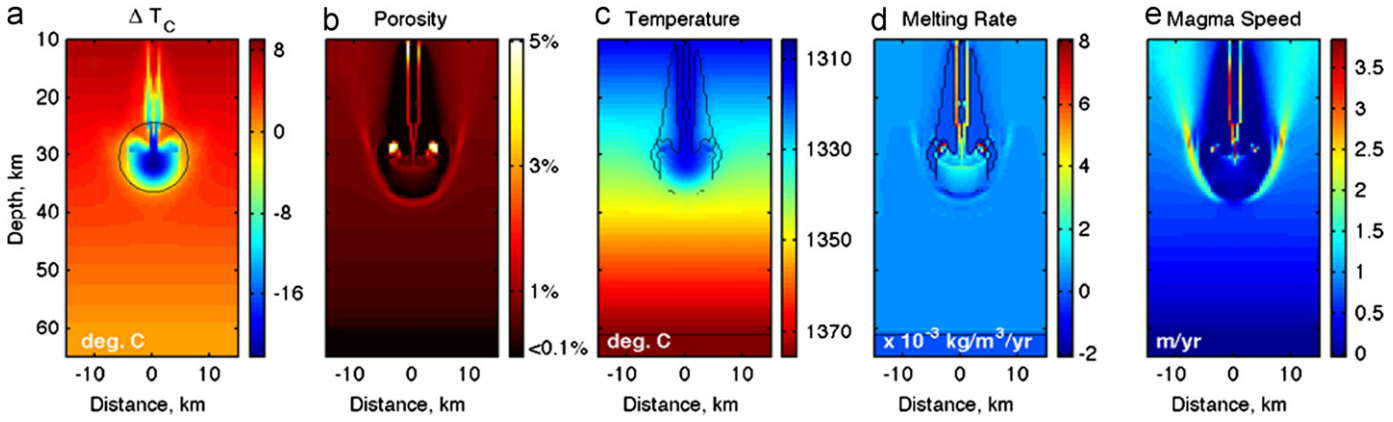

Fig. 5. Output fields from a column model with an enriched heterogeneity. The simulated domain is wider and deeper than the region shown in the figure. The heterogeneity is enriched by 12 wt.%, giving an initial solidus temperature-difference of $\Delta T_C = 50$ °C. The column is upwelling at 3.5 cm/a; melting of the enriched blob begins below the depth of the solidus of the ambient mantle. (a) The solidus difference ΔT_C due to mantle composition. Negative values indicate fertile mantle with a lower solidus temperature than the ambient mantle in °C. Black circle indicates the initial size of the heterogeneity (it has been transposed vertically by a distance $W_0 t$, where t is the elapsed model time). (b) Colours show volume per cent of magma. Black indicates porosities less than 0.1%. (c) The real temperature field in °C. The edge of the partially molten region is marked with by a black line. (d) The melting rate in g/m^3/yr. Black lines as in panel c. (e) The magnitude of the magma velocity $|\mathbf{v}_m|$ in m/yr. The grid-spacing is 0.5 km in this simulation. (For interpretation of the references to colour in this figure caption, the reader is referred to the web version of this article.)

with time that is not due to mantle decompaction. The melting rate in simulations is determined as a part of the solution, and arises from the interplay of the phase diagram, thermodynamic parameters, the flow field, and the thermal structure.

The rate of magmatic flow $|\mathbf{v}_f|$ is shown in Fig. 4b and d. Since buoyancy is the dominant driver of magmatic flow, this rate is typically close to the vertical component of velocity. However, regions with permeability barriers to vertical flow can deflect magma laterally (Sparks and Parmentier, 1991; Spiegelman, 1993). Tracer particles in the supplementary movies provide the clearest demonstration of the evolving flow-pathways in the system. Channelised flow is easily distinguished in Fig. 4b and d by the associated large magmatic flow rates. Channelised melts are transported at higher permeability, and therefore they ascend faster than melt in low-porosity regions between channels. Fig. 4b and c shows that channels extending from heterogeneities have magmatic upwelling rates of just under 10 m/yr. Because channel width (and hence, for a given magmatic throughput, channel porosity) is limited by the grid spacing, simulations at higher resolution yield narrower channels with larger porosity and higher flow speeds. With sufficiently high resolution, it may be possible to reconcile geochemical (e.g. Lundstrom et al., 2000; Stracke et al., 2003) and geological (e.g. Maclennan et al., 2002) constraints on magmatic ascent rates with those predicted by the present theory. At some small length-scale, chemical dispersion (Spiegelman et al., 2001) or local exhaustion of pyroxene from the residue (Liang et al., 2010) may yield a lower limit to channel width.

3.2. Upwelling-column models

To elucidate the melting behaviour of a fertile mantle heterogeneity, we consider the simpler scenario of a column of mantle rock that is upwelling without large-scale shear, as shown in Fig. 5. This is described by a mantle velocity field composed of a local compaction rate plus a constant upwelling rate W_0

(e.g. Spiegelman et al., 2001). To construct the initial composition field, we superimpose a disk of fertile composition onto the column at a depth where the fertile material is unmolten. This heterogeneity upwells with speed W_0 and begins to melt at depths below the ambient melting regime. Eventually, a permeable pathway between the fertile region and the ambient melting regime emerges. Magma then drains upward from the fertile region and infiltrates the ambient mantle, causing reactive melting.

The rate of reactive melting increases with the vertical flux of magma (Hewitt, 2010). Channelisation occurs when this rate is sufficiently large, though we do not have a theory for the stability of diffuse flow in this context. Fig. 5 shows an unstable situation: the excess magmatic flux from the heterogeneity causes intensified local melting, leading to channelised transport. The fertile composition of the magma produced within the heterogeneity reacts with the overlying mantle and reduces its melting temperature—hence the channel is at a lower temperature than the adjacent mantle, as shown in Fig. 5c. This temperature gradient drives a diffusive flux of heat into the channel, powering continued melting, and suppressing melting in the surrounding mantle. The temperature within the channel is fixed at the solidus temperature, which is lower than that of the ambient mantle because of the presence of fertile-sourced magma. The combination of high magmatic flux, fertile composition, reduced temperature, and enhanced melting keep the channel open. Exhaustion of pyroxene from the residue within the channel would modify these dynamics (Liang et al., 2010), however the present calculations do not include multiple solid phases and hence do not capture this modification.

Under what conditions can a fertile heterogeneity cause channelised flow? Fig. 6a shows an ensemble of calculations for different values of disk radius and fertility (expressed in terms of ΔT_C), for an upwelling rate of 3.5 cm/a. As should be expected, channelisation is favoured for larger and more fertile disks. Both of these correspond to a larger excess melt supply at the base of the ambient melting region. If channelisation occurred above a simple threshold of injected melt volume, we might expect the boundary between channelised and unchannelised cases to scale as $-\Delta T_C \propto r^{-2}$. This assumes that melt is formed entirely due to decompression, and that all the melt produced in the heterogeneity is available to create a single channel. Neither of these assumptions holds here, and hence it is not surprising to see more complexity in the shape of the boundary between regimes. Despite this, our models predict that only a modest enrichment is required to nucleate a channel. We can infer that an embedded heterogeneity composed of G2 pyroxenite (Pertermann and Hirschmann, 2003), which has a solidus that is at least 145 °C cooler than peridotite, would be associated with channelised melt transport, whether the melt was derived from the recycled crust itself, or from a hybrid pyroxenite produced by reaction with surrounding peridotite (Yaxley and Green, 1998). A more detailed exploration of the parameters controlling channelisation and channelised transport are provided by Weatherley and Katz (2012).

4. Model approximations and limitations

The results above arise within a theoretical/computational framework that is a simplified and discretised model of magma/mantle interaction in the presence of mantle heterogeneity. In our simulations, channels tend to evolve to a width equal to the grid spacing, indicating that the physics of channelisation is not fully resolved. This seems to be a common feature of energy-conserving equilibrium transport simulations (Hewitt, 2010; Katz and Worster, 2008) and requires further consideration. Fig. 6b shows the results of a resolution test on the column model, which indicates that the simulated patterns of flow are stable relative to the chosen grid-spacing. Visual comparison of the patterns of magmatic flow in simulations of a mid-ocean ridge at different grid resolutions suggests that they are robust, even if these simulations contain some channels that localise to the grid spacing.

The dimensionality of current models is another concern. Two-dimensional simulations impose an infinite out-of-plane length on all features of the solution; this restricts the flow of matter and heat to be in-plane, and hence reduces their efficiency.

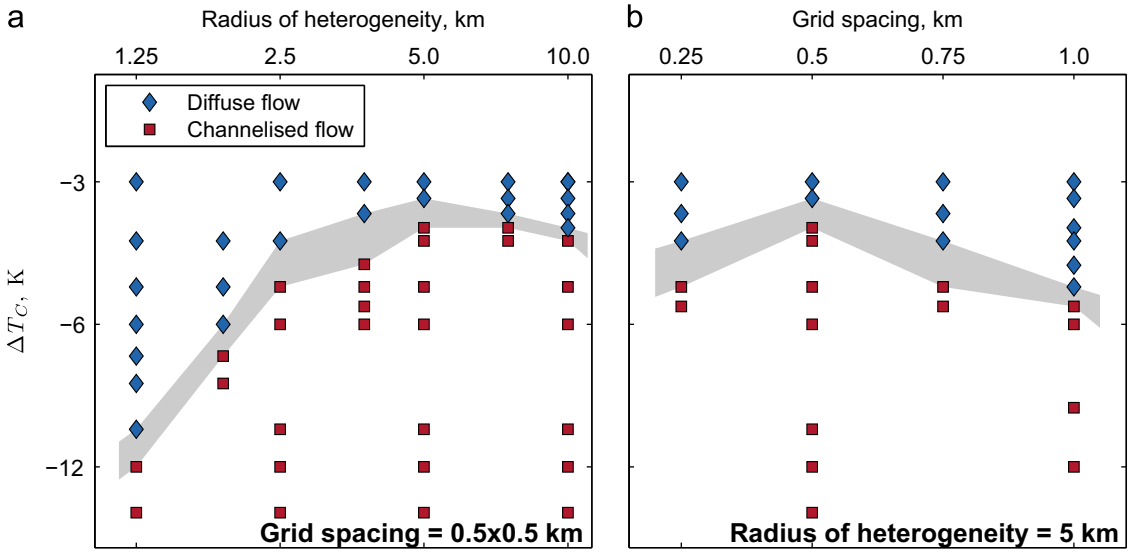

Fig. 6. Regime diagram showing the boundary between diffuse and channelised flow. Each point represents a single simulation; each has an upwelling rate of 3.5 cm/a. Red squares indicate that a channel formed as melt drained from the heterogeneity; blue diamonds indicate that melt escaped the heterogeneity by diffuse porous flow, and did not induce channelisation. Points within the grey band demonstrate behaviour that is transitional between these two regimes. (a) Melt-migration regime as a function of the parameters that describe the imposed heterogeneity: blob radius and blob fertility (expressed as ΔT_C, the solidus difference due to composition). (b) Melt-migration regime as a function of the grid spacing used for numerical solution. (For interpretation of the references to colour in this figure caption, the reader is referred to the web version of this article.)

If channels associated with fertile heterogeneities take a roughly cylindrical form in three-dimensions, enhanced convergence of magmatic and heat flow might reinforce the channel-forming mechanism. At a larger scale, offsets to the mid-ocean ridge introduce three-dimensional variations in the thermal and flow structure of the mantle beneath. This probably affects magmatic transport beneath the lithosphere (e.g. Magde and Sparks, 1997; Hebert and Montési, 2011), and may interact with the heterogeneous mantle in unrecognised ways.

The most important simplification in our theoretical framework is the petrological model. The full thermochemical complexity of the mantle cannot be described by a two-phase, two-component system. For example, Yaxley and Green (1998) note that eclogite can melt to produce quartz-normative magma that reacts with lherzolite to form orthopyroxene. Sobolev et al. (2005) call on this interaction in their model of the formation of hybrid pyroxenites in mantle plumes. They argue that hybrid pyroxenites later melt and transport the geochemical signature of the eclogite to the volcano. The thermochemical system considered in the present paper does not capture reactive precipitation of pyroxene. Nonetheless, the present formulation does capture the variation of mantle solidus with composition, which should approximately apply to the hybrid pyroxenite produced by the precipitation reaction. Furthermore, present models are built on an energetically consistent description of decompression and reactive melting. These are fundamental to the context for basalt petrogenesis, and hence should provide a sufficient foundation for dynamical models. In the future work, extensions of the present models will include (a) tracking two solid phases, olivine and orthopyroxene, with the associated incongruent melting reactions, and (b) incorporating volatiles into the thermochemical system as a third chemical component.

In preceding two-phase computational models of mid-ocean ridges, magma was extracted from the domain through an internal boundary condition representing a "dike" that extends into the partially molten mantle beneath the ridge axis (Katz, 2010). This approach creates a variety of computational issues when coupled with a heterogeneous melt distribution. Hence in the current model formulation, magma is not allowed to escape the domain at all; this means that magma pools beneath the ridge axis (and within fertile blobs, and at the base of the lithosphere), locally reaching porosities up to 100%. High porosity violates two of the assumptions used in deriving the force-balance governing equations: that the porosity is everywhere below the limiting porosity for disaggregation of the solid matrix, and that the deviatoric stresses on the magma cancel out such that magmatic flow is governed by Darcy's law. However, the resulting model is computationally tractable and, outside of the localised regions where the porosity is high, it is entirely consistent with the relevant physical assumptions.

The presence of regions of high porosity causes two problems, both of which are addressed by modifying the constitutive relationships. First, since the shear viscosity of the magma/mantle aggregate is an exponentially decreasing function of porosity (Kelemen et al., 1997), regions with large porosity have very low shear viscosity. This can lead to the breakdown of convergence of the numerical algorithms used to solve for mantle flow. To avoid this difficulty, we impose a minimum viscosity of 10^{15} Pa s by adding this number (appropriately non-dimensionalised) onto the viscosity calculated by the relevant constitutive law (Katz, 2010). The dynamic range of viscosity in the simulations still spans 10 orders of magnitude, so the gross behaviour of the simulations is not modified. The second problem is that the constitutive law for permeability as a function of porosity yields very large results at high porosity, which can give rise to convective flow within the melt pools at speeds of hundreds of metres per year. These melt-pool localised flows are irrelevant for the present investigation, and yet they drastically reduce the size of the time-step in simulations. To avoid this, we impose an upper limit on the permeability, corresponding to a maximum porosity of 10%.

If the minimum viscosity and maximum permeability have an effect on melt transport outside the high-porosity melt pools, it is to diminish channelisation, rather than promote it. The key driver of channelisation is the melt flux through the mantle matrix. The upper limit on permeability and the lower limit on viscosity both increase the resistance to flow within a melt pool relative to a non-limited case, and hence they increase the pressure gradient required to drive magma out of the melt pool into the ambient mantle. Theory suggests that this is unimportant, because the lower porosity and permeability in the mantle around a melt pool are rate-limiting. Furthermore, sensitivity tests show no appreciable difference from our reference models that are shown in figures here. The effect of these model restrictions seems to be confined to within the melt pools.

5. Discussion

The comparison between two hypothetical styles of mantle heterogeneity, illustrated in Figs. 3 and 4, indicates that the emergence of channels is not very sensitive to the spatial distribution of heterogeneity. In the first case (Figs. 3 and 4, left column), the uniform, isolated, fertile blobs are intended to represent enclaves of recycled oceanic crust that melt preferentially to the ambient mantle. They are assumed to be large enough that they can be individually resolved by the simulation. It is also possible, however, that recycled crust is so efficiently stirred or reacted back into the mantle that it is present as bodies with a minimum dimension smaller than the 1 km grid-resolution of present simulations. This type of heterogeneity is better represented as being ubiquitous, with a spatially variable concentration, as it appears in the second case (Figs. 3 and 4, right column). Here the noise field is a discrete representation of a continuous variation in two spatial dimensions. With sufficiently large amplitude of heterogeneity, both of these styles of heterogeneity develop high-porosity channels with rapid rates of melt segregation. The column models summarised in Fig. 6 quantify the amplitude criterion, as a function of the size of heterogeneity. The results depend on the compaction length of the ambient mantle, and thermodynamic parameters such as the Clapeyron slope, solidus slope, and latent heat. The sensitivities to these parameters are considered by Weatherley and Katz (2012).

For a more quantitative understanding of melting in the present simulations, it is helpful to consider a simple, analytical expression for the melting rate. This expression can be obtained by neglecting thermal and compositional diffusion and assuming steady-state conditions to obtain (Hewitt, 2010)

$$\Gamma = -\rho \overline{\mathbf{v}} \cdot \hat{\mathbf{g}} \left(\frac{\rho g/\gamma - \alpha g \mathcal{T}_0/c}{M\Delta C + L/c} \right), \tag{1}$$

where $\overline{\mathbf{v}} = \phi \mathbf{v}_f + (1-\phi)\mathbf{v}_m$ is the phase averaged velocity, $\hat{\mathbf{g}}$ is a unit-vector in the direction of gravity, and the rest of the symbols represent thermodynamic parameters that are given in Table 1. Eq. (1) states that melting is driven by the phase-averaged vertical mass flux. The contribution of the solid phase is a standard expression for the decompression melting rate (e.g. Asimow et al., 1997), while the contribution by the magma represents reactive melting in an equilibrium formulation (Hewitt, 2010). For comparison, the reactive melting rate in models that neglect conservation of energy (e.g. Liang et al., 2010) is

$$\Gamma_R = \frac{\rho \phi w}{\Delta C} \frac{\rho g/\gamma}{M},$$

where w is the magmatic upwelling rate. This latter equilibrium formulation excludes decompression melting, an omission that is known to destabilise the system to channels (Spiegelman et al., 2001; Hewitt, 2010). A version of Eq. (1) augmented to account for the contribution of thermal and chemical diffusion is presented by Weatherley and Katz (2012).

Eq. (1) states that locations with a larger flux of magma will melt more rapidly than locations with a smaller flux. Melting increases porosity and permeability, and hence allows for an even greater flux of magma. Channels form as a result of this feedback. At the same time, melting converts sensible heat to latent heat, and so the availability of energy limits the rate at which melting can progress. This is why accounting for conservation of energy acts to suppress channelisation, and why Hewitt (2010) found that channelisation in a homogeneous upwelling column requires an unrealistically low value for the latent heat of melting. However, the introduction of heterogeneities changes this picture. Fertile enclaves of recycled oceanic crust melt at a lower temperature than the ambient, refractory mantle. In our simulations, the localised excess melt derived from heterogeneities increases melting according to Eq. (1) and this leads to channel formation. Channels bearing magma that is derived from fertile heterogeneities are cooler than their surroundings. Heat therefore diffuses inward, supplying energy to be converted from sensible to latent heat. Our models predict that heat diffusion powers melting within channels (see also Weatherley and Katz, 2012). This line of argument, considered in light of the findings of Hewitt (2010), suggests that mantle heterogeneity may actually be a necessary condition for channelised flow.

Regardless of whether it is necessary to explain channelisation, mantle heterogeneity is present in the source regions of MORB, both in terms of recycled lithologies that upwell with the ambient mantle, and in terms of spatial variations of pyroxene content. As we have shown here, variations in mantle fertility could have a drastic effect on the pattern of melting and melt transport within the sub-ridge melting regime. The results of current simulations are probably more realistic than the concept of uniform melt extraction from a homogeneous mantle (as modelled by, for example, Katz, 2010). The variations in melting rate that are imposed by the heterogeneity structure of the upwelling mantle are likely to be much larger than the infinitesimal noise (e.g. Spiegelman et al., 2001) or coherent perturbations (Spiegelman and Kelemen, 2003; Liang et al., 2010; Schiemenz et al., 2011) used to seed prior simulations of channelised flow. If this is the case, then patterns of melt-flow arising from the heterogeneity structure would overprint or even exclude evanescent features such as compaction–dissolution waves (Aharonov et al., 1995; Hesse et al., 2011).

Although details of the spatial distribution of mantle heterogeneity do have an effect in our calculations, the formation of channelised, heterogeneous, and time-dependent patterns of magmatic flux seems to be a robust outcome of models. This depends on the presence of a sufficiently large amplitude of variation in solidus temperature at sufficiently small length-scales of variation within the melting region. The differences in model results between our two scenarios for mantle heterogeneity arise from the topological structure of the heterogeneity. Isolated fertile blobs tend to produce narrower channels that traverse the refractory ambient mantle, while the smoothly varying random-noise field yields a flow structure that interconnects fertile regions with zig-zagging channels. In the mantle, heterogeneity may take the form of vertically oriented veins that, during melting, would become high-permeability pathways for melt transport. In this case, one would expect a strong geochemical signature of eclogite/pyroxenite melts; in contrast, what has been observed indicates participation of a hybrid pyroxenite/peridotite (Sobolev et al., 2007; Shorttle and Maclennan, 2011). Regardless, neither of the present hypotheses for mantle heterogeneity explicitly models enhanced transport by vertical veins, nor do they capture the small length-scales of lithological variation that are expected in the mantle.

Beyond such considerations, the simulated mantle heterogeneity in our mid-ocean ridge models (Fig. 3) has consequences for melt focussing to the ridge axis. Previous models that consider a homogeneous mantle predict focussing by flow through a sloping channel along the base of the thermal boundary layer (Sparks and Parmentier, 1991; Ghods and Arkani-Hamed, 2000; Hebert and Montési, 2010). This style of focussing is evident over narrow intervals in Fig. 3 and associated movies. A broader focussing of magma is interrupted by the presence of high-porosity melt pools that modify the thermal structure and trap locally produced melt, which prevents it from reaching the ridge axis. Such melt trapping was previously noted in simulations for a homogeneous mantle with low viscous resistance to compaction (Katz, 2008); here, however, the bulk viscosity is large (2×10^{19} Pa s) and hence heterogeneity must be the controlling factor.

In the present models, the simulated melt pools cool and solidify in place at the base of the lithosphere, leading to refertilisation of the mantle by recrystallised blobs (Fig. 3a and c); this may represent a mechanism for generating mantle heterogeneity in the mantle lithosphere. Halliday et al. (1995) invoked this process to metasomatise the lithosphere with enriched melts produced at low melt-fraction. In their model, this metasomatised lithosphere is recycled into the source regions of MOR and hotspot magmas, to explain observed trace-element ratios. Donnelly et al. (2004) argued for a similar mechanism for the genesis of enriched MORB, where mantle metasomatised by low-degree melts of subducting slabs is recycled into the source region beneath a ridge. Our simulations display mantle refertilisation by melts generated at a range of melt fractions. Extension of simulations with an explicit model of trace-element transport is required to make quantitative comparison with predictions by Halliday et al. (1995).

Observations of the oceanic crust and lithosphere by seismic refraction (Durant and Toomey, 2009) and reflection (Canales et al., 2009, 2012) indicate the presence of off-axis magma bodies in the mid and lower crust at distances up to ~ 20 km from the ridge axis. If these magma bodies were emplaced at the ridge axis, cooling by hydrothermal circulation and conduction should have caused them to solidify before reaching such distances. In contrast, if the imaged magma bodies are fed by dikes or channels that tap melt from pools at the bottom of the thermal boundary layer, one should expect them to be younger and hotter than the surrounding crust. Models presented here exclude hydrofracture and hence cannot capture the transport of magma across the thermal boundary layer. It seems plausible, however, that sub-lithospheric melt pools predicted by present models could supply magma to off-axis chambers within the crust, and could act as a source for off-axis volcanism. This speculation might be testable against geochemical observations of off-axis lavas erupted at seamounts and against geological observations of ophiolites.

Mantle heterogeneity may also have magmatic effects at much greater distances from the ridge axis. Possible evidence for this comes from Harmon et al. (2011), who used Rayleigh wave tomography to image the mantle lithosphere and asthenosphere beneath the Pacific plate, west of the EPR. Harmon et al. (2011) invoke small-scale convection driven by mantle heterogeneity to explain the gravitational and seismic signature beneath prominent volcanic lineaments that trend away from the ridge axis. These features are at a larger scale than the heterogeneity considered in the present simulations, but the concept of convective mantle flow associated with lateral variations in melting

is supported by present models (see esp. Appendix B), as well as past work by Raddick et al. (2002), for example.

6. Summary and conclusions

Despite these limitations, by accounting for melting and magmatic transport in the context of conservation of mass, momentum, and energy, our simulations provide a physically consistent, fluid-dynamical perspective on the consequences of mantle heterogeneity. They reconcile salient features from geochemical and field studies, as well as previous theory. Our results show that magmatic segregation can generate chemical heterogeneity at the base of the lithosphere by melt pooling and crystallisation; these pools may supply magma to off-axis crustal magma chambers. The results also show that fertile heterogeneities may nucleate high-flux magmatic channels that are cooler than the surrounding mantle. Diffusion of heat into fertile heterogeneities and their attendant magmatic channels can boost melting there, and can suppress melting in the adjacent rock. These results establish a physical connection between compositional heterogeneity in the mantle and channelised magmatic transport beneath mid-ocean ridges, though such a connection has previous been inferred based on geochemistry (Lundstrom et al., 2000; Kogiso et al., 2004). Channelised flow is regarded as a primary mechanism for generating the lithological variability observed in the mantle section of ophiolites (e.g. Kelemen et al., 1995; Braun and Kelemen, 2002), and is thought to influence the uranium-series disequilibria (e.g. Spiegelman and Kelemen, 2003; Elliott and Spiegelman, 2003) and orthopyroxene-undersaturation (e.g. Kelemen et al., 1995) of mid-ocean ridge basalts. While the results presented here may be consistent with these observations, more work is required to understand and refine predictions, and to validate the model through comparison with observations.

Acknowledgements

The authors thank the Oxford Supercomputing Centre for cluster-time and computing support, D. Ketcheson and V. Titarev for advice on TVD advection schemes, G. Ito, C. Langmuir, and I. Hewitt for stimulating discussions, and D. Pyle for comments on the manuscript. Constructive reviews by J. Maclennan and an anonymous reviewer helped us to substantially improve the manuscript. This work was supported by grant NE/H00081X/1 from the UK Natural Environment Research Council and a Research Councils UK fellowship for Katz.

Appendix A. Stochastic hypotheses for mantle heterogeneity

This appendix describes the two algorithms used to generate hypothetical mantle heterogeneity fields, such as those shown in Fig. 2. For clarity of exposition, we exclude some of the details here; the MATLAB implementation of these methods is available by email request to Katz.

Both algorithms begin with an array of random phase angles φ_{jk}, and an array of discrete wavenumbers $\boldsymbol{\kappa}_{jk}$. The wavenumbers are used to create an array of mode-amplitudes A_{jk}. Phase angles and amplitudes are combined and transformed from Fourier into Cartesian space using

$$\chi_{jk} = \mathrm{Re}\{\mathcal{F}^{-1}[A_{jk}\exp(i\varphi_{jk})]\}, \tag{2}$$

where $\mathcal{F}^{-1}$ is the inverse discrete Fourier transform, Re denotes the real part, and multiplication is performed component-wise, with no summation. The algorithms differ in the rule for generating A_{jk} and how they process χ_{jk} once it has been obtained. For a given algorithm and set of control parameters, each instantiation of the random phase array will produce a different output field.

Random noise Both algorithms begin with an array $\kappa_{jk} = \sqrt{k_x^2 + k_z^2}$ of wavenumbers. Each component of the wave-vector is given by $k_i = 2\pi n/L_i$ where L_i is the maximum distance in the i-direction ($i = x,z$), n is an integer ranging from $-N_i/2$ to $N_i/2$, and N_i is the number of grid cells in the i-direction. An amplitude array is constructed using a band-pass filter on the magnitude of discrete wavenumbers

$$A_{jk} = \frac{1}{2}\left[1 - \tanh\left(\frac{|\kappa_{jk}| - |\kappa|_{\max}}{\sigma}\right)\right],$$

where $|\kappa|_{\max}$ is the desired cutoff on the magnitude of the wave-vector and σ is a parameter controlling the sharpness of the cutoff. This filter removes smaller wavelengths of oscillation. In the mantle, solid-state diffusion would damp oscillations with wavelengths λ on the decimetre scale (Hofmann and Hart, 1978); here we damp small wavelengths that would be lost to numerical diffusion. We take $|\kappa|_{\max} = 2\pi/\lambda_{\min}$, where the minimum wavelength is set to be a small multiple of the grid spacing. This recipe gives equal variation at wavelengths larger than $\lambda_{\min}$.

Random blobs The random blob algorithm goes one step further, converting the continuous variation produced by the RN algorithm into a binary composition of fertile blobs surrounded by depleted rock. For a target mantle composition that is 10% fertile blobs by volume, a cutoff value χ_{cut} is determined such that the number of array entries with $\chi_{jk} > \chi_{\mathrm{cut}}$ is one-tenth of total number of entries in χ_{jk}. Entries of χ_{jk} above this threshold are set to unity, entries equal or below are set to zero.

The minimum size of the blobs is controlled by the choice of $\lambda_{\min}$.

For both algorithms, the resultant composition field is prescribed as

$$C_{jk} = C_0 - \chi_{jk} C_*,$$

where C_* is the desired amplitude of compositional variation.

Appendix B. Movies

The ridge simulations described in the manuscript are shown as animations in four movies. The first set of movies (Movies 1 and 2, see Supplementary material) shows the porosity ϕ and compositional solidus perturbation ΔT_C, while the second set (Movies 3 and 4, see Supplementary material) shows the potential temperature $\mathcal{T}$ and the magmatic flow speed $|\mathbf{v}_f|$.

Appendix C. Summary of numerical methods

A nearly complete description of the numerical methods used in the present simulations was given in previous publications (Katz et al., 2007; Katz, 2008, 2010). Here we consider only differences from previous work. A key difference is the use of a Total Variation Diminishing (TVD) advection scheme with SUPERBEE limiter. A fully referenced discussion of this scheme in the context of geodynamic calculations is given by Šrámek et al. (2010). TVD schemes are useful where the advected field has sharp jumps between regions of smooth variation. Typical second-order

advection schemes are dispersive in such cases, but TVD schemes effectively capture and advect these jumps. This feature is crucial for advecting discrete blobs of fertile, solid mantle through the domain. These blobs have nearly uniform composition in their interior, but sharp jumps at their edges. A dispersive advection scheme would produce spurious oscillations of bulk concentration adjacent to jumps that would have a drastic effect on the melting behaviour of the system. With a TVD scheme, this problem is avoided. The scheme has second-order accuracy in regions of smooth variation and first-order accuracy at jumps.

Another important difference is the use of explicit time-stepping for the equations governing bulk enthalpy and composition. The sharp gradients in composition and porosity that occur in present models create convergence problems in the nonlinear (Newton) iteration required by implicit methods. Such problems can be attributed to nonlinearity of the Enthalpy Method, especially near the solidus temperature. Explicit time steps avoid such problems, but reduce the accuracy of the method. Comparison with limited simulations run with semi-implicit time-stepping shows that differences in the results are quantitatively insignificant for present purposes. In the simulation of MOR solid flow and melt migration, all time-steps are computed explicitly, while for the magmatic column calculations, an explicit step is taken only when an implicit step fails to converge. The fraction of explicit time-steps in the column model is typically less than 10%. In the mid-ocean ridge simulations, we further accelerate the code by staggering the computationally expensive update of slowly evolving variables (dynamic pressure P and mantle flow $\mathbf{v}_m$) to every $\sim$third time-step.

Appendix D. Supplementary material

Supplementary data associated with this article can be found in the online version of http://dx.doi.org/10.1016/j.epsl.2012.04.042.

References

Aharonov, E., Whitehead, J., Kelemen, P., Spiegelman, M., 1995. Channeling instability of upwelling melt in the mantle. J. Geophys. Res.—Solid Earth 100, 20433–20450.

Allègre, C.J., Turcotte, D.L., 1986. Implications of a two-component marble-cake mantle. Nature 323 (6084), 123–127.

Asimow, P., Hirschmann, M., Stolper, E., 1997. An analysis of variations in isentropic melt productivity. Philos. Trans. R. Soc. London A 355 (1723), 255–281.

Balay, S., Brown, J., Buschelman, K., Gropp, W.D., Kaushik, D., Knepley, M.G., McInnes, L.C., Smith, B.F., Zhang, H., 2011. PETSc Web Page. URL 〈http://www.mcs.anl.gov/petsc〉.

Batchelor, G., 1967. An Introduction to Fluid Mechanics. Cambridge University Press.

Braun, M., Kelemen, P.B., 2002. Dunite distribution in the Oman ophiolite: implications for melt flux through porous dunite conduits. Geochem. Geophys. Geosyst. 3, 8603.

Canales, J.P., Carton, H., Carbotte, S.M., Mutter, J.C., Nedimović, M.R., Xu, M., Aghaei, O., Marjanović, M., Newman, K., 2012. Network of off-axis melt bodies at the East Pacific Rise. Nat. Geosci. 5, 279–283, http://dx.doi.org/10.1038/NGEO1377.

Canales, J.P., Nedimovic, M.R., Kent, G.M., Carbotte, S.M., Detrick, R.S., 2009. Seismic reflection images of a near-axis melt sill within the lower crust at the Juan de Fuca ridge. Nature 460 (7251), 89–94.

Davies, G.F., 2009. Reconciling the geophysical and geochemical mantles: plume flows, heterogeneities, and disequilibrium. Geochem. Geophys. Geosyst. 10 (10).

Donnelly, K.E., Goldstein, S.L., Langmuir, C.H., Spiegelman, M., 2004. Origin of enriched ocean ridge basalts and implications for mantle dynamics. Earth Planet. Sci. Lett. 226 (3–4), 347–366.

Durant, D.T., Toomey, D.R., 2009. Evidence and implications of crustal magmatism on the flanks of the East Pacific Rise. Earth Planet. Sci. Lett. 287, 130–136.

Elliott, T., Spiegelman, M., 2003. Melt migration in oceanic crustal production: a U-series perspective. In: Holland, H.D., Turekian, K. (Eds.), The Crust. Treatise on Geochemistry, vol. 3. Elsevier-Pergamon, pp. 465–510.

Farnetani, C.G., Hofmann, A.W., 2009. Dynamics and internal structure of a lower mantle plume conduit. Earth Planet. Sci. Lett. 282, 314–322.

Ghods, A., Arkani-Hamed, J., 2000. Melt migration beneath mid-ocean ridges. Geophys. J. Int. 140, 687–697.

Gurnis, M., 1986. Quantitative bounds on the size spectrum of isotopic heterogeneity within the mantle. Nature 323 (6086), 317–320.

Halliday, A.N., Lee, D.-C., Tommasini, S., Davies, G.R., Paslick, C.R., Godfrey Fitton, J., James, D.E., 1995. Incompatible trace elements in OIB and MORB and source enrichment in the sub-oceanic mantle. Earth Planet. Sci. Lett. 133 (3–4), 379–395.

Harmon, N., Forsyth, D., Weeraratne, D., Yang, Y., Webb, S., 2011. Mantle heterogeneity and off axis volcanism on young Pacific lithosphere. Earth Planet. Sci. Lett. 311 (3), 306–315.

Hauri, E., 1996. Major-element variability in the Hawaiian mantle plume. Nature 382 (6590), 415–419.

Hebert, L.B., Montési, L.G.J., 2010. Generation of permeability barriers during melt extraction at mid-ocean ridges. Geochem. Geophys. Geosyst. 11 (12), Q12008.

Hebert, L.B., Montési, L.G.J., 2011. Melt extraction pathways at segmented oceanic ridges: application to the East Pacific rise at the Siqueiros transform. Geophys. Res. Lett. 38 (11).

Helffrich, G.R., Wood, B.J., 2001. The Earth's mantle. Nature 412 (6846), 501–507.

Hesse, M., Schiemenz, A., Liang, Y., Parmentier, E., 2011. Compaction–dissolution waves in an upwelling melting column. Geophys. J. Int. 187 (3), 1057–1075.

Hewitt, I.J., 2010. Modelling melting rates in upwelling mantle. Earth Planet. Sci. Lett. 300, 264–274.

Hier-Majumder, S., Ricard, Y., Bercovici, D., 2006. Role of grain boundaries in magma migration and storage. Earth Planet. Sci. Lett. 248, 735–749.

Hirschmann, M.M., Stolper, E.M., 1996. A possible role for garnet pyroxenite in the origin of the "garnet signature" in MORB. Contrib. Mineral. Pet. 124 (2), 185–208.

Hofmann, A., Hart, S., 1978. An assessment of local and regional isotopic equilibrium in the mantle. Earth Planet. Sci. Lett. 38, 44–62.

Hofmann, A., White, W., 1982. Mantle plumes from ancient oceanic crust. Earth Planet. Sci. Lett. 57 (2), 421–436.

Ito, G., Mahoney, J., 2005. Flow and melting of a heterogeneous mantle. 2. Implications for a chemically nonlayered mantle. Earth Planet. Sci. Lett. 230 (1–2), 47–63.

Jull, M., Kelemen, P., Sims, K., 2002. Consequences of diffuse and channelled porous melt migration on uranium series disequilibria. Geochim. Cosmochim. Acta 66, 4133–4148.

Katz, R., 2008. Magma dynamics with the enthalpy method: benchmark solutions and magmatic focusing at mid-ocean ridges. J. Pet. 49, 2099–2121, http://dx.doi.org/10.1093/petrology/egn058.

Katz, R., 2010. Porosity-driven convection and asymmetry beneath mid-ocean ridges. Geochem. Geophys. Geosyst. 10, Q0AC07, http://dx.doi.org/10.1029/2010GC003282.

Katz, R., Knepley, M., Smith, B., Spiegelman, M., Coon, E., 2007. Numerical simulation of geodynamic processes with the portable extensible toolkit for scientific computation. Phys. Earth Planet. Int. 163, 52–68.

Katz, R.F., Rudge, J.F., 2011. The energetics of melting fertile heterogeneities within the depleted mantle. Geochem. Geophys. Geosyst. 12 (10), Q0AC16, http://dx.doi.org/10.1029/2011GC003834.

Katz, R.F., Worster, M.G., 2008. Simulation of directional solidification, thermochemical convection, and chimney formation in a Hele-Shaw cell. J. Comput. Phys. 227, 9823–9840, http://dx.doi.org/10.1016/j.jcp.2008.06.039.

Kelemen, P., Hirth, G., Shimizu, N., Spiegelman, M., Dick, H., 1997. A review of melt migration processes in the adiabatically upwelling mantle beneath oceanic spreading ridges. Philos. Trans. R. Soc. London. A 355 (1723), 283–318.

Kelemen, P., Shimizu, N., Salters, V., 1995. Extraction of mid-ocean-ridge basalt from the upwelling mantle by focused flow of melt in dunite channels. Nature 375 (6534), 747–753.

Kogiso, T., Hirschmann, M., Reiners, P., 2004. Length scales of mantle heterogeneities and their relationship to ocean island basalt geochemistry. Geochim. Cosmochim. Acta 68 (2), 345–360.

Liang, Y., Schiemenz, A., Hesse, M.A., Parmentier, E.M., 2011. Waves, channels and the preservation of chemical heterogeneities during melt migration in the mantle. Geophys. Res. Lett. 38 (20).

Liang, Y., Schiemenz, A., Hesse, M.A., Parmentier, E.M., Hesthaven, J.S., 2010. High-porosity channels for melt migration in the mantle: top is the dunite and bottom is the harzburgite and lherzolite. Geophys. Res. Lett. 37 (15), L15306.

Lundstrom, C., Gill, J., Williams, Q., 2000. A geochemically consistent hypothesis for MORB generation. Chem. Geol. 162 (2), 105–126.

Maclennan, J., 2008. Lead isotope variability in olivine-hosted melt inclusions from Iceland. Geochim. Cosmochim. Acta 72 (16), 4159–4176.

Maclennan, J., Jull, M., McKenzie, D., Slater, L., Grönvold, K., 2002. The link between volcanism and deglaciation in Iceland. Geochem. Geophys. Geosyst. 3, 1062.

Magde, L., Sparks, D., 1997. Three-dimensional mantle upwelling, melt generation, and melt migration beneath segment slow spreading ridges. J. Geophys. Res.—Solid Earth 102, 20571–20583.

McKenzie, D., 1984. The generation and compaction of partially molten rock. J. Pet. 25 (3), 713–765.

Morgan, Z., Liang, Y., 2003. An experimental and numerical study of the kinetics of harzburgite reactive dissolution with applications to dunite dike formation. Earth Planet. Sci. Lett. 214 (1–2), 59–74.

Pertermann, M., Hirschmann, M., 2003. Partial melting experiments on a MORB-like pyroxenite between 2 and 3 GPa: constraints on the presence of

pyroxenite in basalt source regions from solidus location and melting rate. J. Geophys. Res.—Solid Earth 108 (B2), 2125.
Raddick, M., Parmentier, E., Scheirer, D., 2002. Buoyant decompression melting: a possible mechanism for intraplate volcanism. J. Geophys. Res.—Solid Earth 107.
Ribe, N., 1985. The generation and composition of partial melts in the Earth's mantle. Earth Planet. Sci. Lett. 73, 361–376.
Richter, F.M., Daly, S.F., 1989. Dynamical and chemical effects of melting a heterogeneous source. J. Geophys. Res.—Solid Earth 94 (B9), 12499–12510.
Ritsema, J., Xu, W., Stixrude, L., Lithgow-Bertelloni, C., 2009. Estimates of the transition zone temperature in a mechanically mixed upper mantle. Earth Planet. Sci. Lett. 277, 244–252.
Rudge, J., Bercovici, D., Spiegelman, M., 2010. Disequilibrium melting of a two phase multicomponent mantle. Geophys. J. Int. 184, 699–718.
Schiemenz, A., Liang, Y., Parmentier, E.M., 2011. A high-order numerical study of reactive dissolution in an upwelling heterogeneous mantle. I. Channelization, channel lithology and channel geometry. Geophys. J. Int., 1–24.
Shorttle, O., Maclennan, J., 2011. Compositional trends of Icelandic basalts: implications for short-length scale lithological heterogeneity in mantle plumes. Geochem. Geophys. Geosyst. 12 (11), Q11008.
Sleep, N., 1984. Tapping of magmas from ubiquitous mantle heterogeneities. J. Geophys. Res.—Solid Earth 89 (B12), 10–29.
Sobolev, A., Hofmann, A., Kuzmin, D., Yaxley, G., Arndt, N., Chung, S.-L., Danyushevsky, L., Elliott, T., Frey, F.A., Garcia, M., Gurenko, A., Kamenetsky, V., Kerr, A., Krivolutskaya, N., Matvienkov, V., Nikogosian, I., Rocholl, A., Sigurdsson, I.A., Sushchevskaya, N., Teklay, M., 2007. The amount of recycled crust in sources of mantle-derived melts. Science 316 (5823), 412–417.
Sobolev, A., Hofmann, A., Sobolev, S., Nikogosian, I., 2005. An olivine-free mantle source of Hawaiian shield basalts. Nature 434 (7033), 590–597.
Sparks, D., Parmentier, E., 1991. Melt extraction from the mantle beneath spreading centers. Earth Planet. Sci. Lett. 105 (4), 368–377.
Spiegelman, M., 1993. Physics of melt extraction: theory, implications, and applications. Philos. Trans. R. Soc. London A 342, 23–41.
Spiegelman, M., Kelemen, P., 2003. Extreme chemical variability as a consequence of channelized melt transport. Geochem. Geophys. Geosyst. 4.
Spiegelman, M., Kelemen, P., Aharonov, E., 2001. Causes and consequences of flow organization during melt transport: the reaction infiltration instability in compatible media. J. Geophys. Res.—Solid Earth 106 (B2), 2061–2077.
Stracke, A., Bourdon, B., 2009. The importance of melt extraction for tracing mantle heterogeneity. Geochim. Cosmochim. Acta 73 (1), 218–238.
Stracke, A., Bourdon, B., McKenzie, D., 2006. Melt extraction in the Earth's mantle: constraints from U–Th–Pa–Ra studies in oceanic basalts. Earth Planet. Sci. Lett. 244, 97–112.
Stracke, A., Zindler, A., Salters, J.M., McKenzie, D., Grönvold, K., 2003. The dynamics of melting beneath Theistareykir, northern Iceland. Geochem. Geophys. Geosyst. 4 (10).
Šrámek, O., Ricard, Y., Dubuffet, F., 2010. A multiphase model of core formation. Geophys. J. Int. 181 (1), 198–220.
Weatherley, S.M., Katz, R.F., 2012. Melting and channelized magmatic flow in chemically heterogeneous, upwelling mantle. Geochem. Geophys. Geosys. 13 (1), Q0AC18, http://dx.doi.org/10.1029/2011GC003989.
Yaxley, G., Green, D., 1998. Reactions between eclogite and peridotite: mantle refertilisation by subduction of oceanic crust. Schweiz. Mineral. Petrogr. Mitt. 78, 243–255.